Topological magnon gap engineering in van der Waals CrI₃ ferromagnets

Verena Brehm [1,*] Pawel Sobieszczyk [2] Jostein N. Kløgetvedt,[1] Richard F. L. Evans [3]
Elton J. G. Santos,[4,5,6] and Alireza Qaiumzadeh [1]

[1]*Center for Quantum Spintronics, Norwegian University of Science and Technology, 7034 Trondheim, Norway*
[2]*Institute of Nuclear Physics Polish Academy of Sciences, Radzikowskiego 152, 31-342 Krakow, Poland*
[3]*School of Physics, Engineering and Technology, University of York, York, YO10 5DD, United Kingdom*
[4]*Institute for Condensed Matter Physics and Complex Systems, School of Physics and Astronomy,
The University of Edinburgh, Edinburgh EH9 3FD, Untied Kingdom*
[5]*Higgs Centre for Theoretical Physics, The University of Edinburgh, EH9 3FD, United Kingdom*
[6]*Donostia International Physics Center (DIPC), 20018 Donostia-San Sebastián, Basque Country, Spain*

The microscopic origin of the topological magnon band gap in CrI₃ ferromagnets has been a subject of controversy for years since two main models with distinct characteristics, i.e., Dzyaloshinskii-Moriya (DM) and Kitaev, provided possible explanations with different outcome implications. Here, we investigate the angular magnetic field dependence of the magnon gap of CrI₃ by elucidating what main contributions play a major role in its generation. We implement stochastic atomistic spin-dynamics simulations to compare the impact of these two spin interactions on the magnon spectra. We observe three distinct magnetic field dependencies between these two gap opening mechanisms. First, we demonstrate that the Kitaev-induced magnon gap is influenced by both the direction and amplitude of the applied magnetic field, while the DM-induced gap is solely affected by the magnetic field direction. Second, the position of the Dirac cones within the Kitaev-induced magnon gap shifts in response to changes in the magnetic field direction, whereas they remain unaffected by the magnetic field direction in the DM-induced gap scenario. Third, we find a direct-indirect magnon band gap transition in the Kitaev model by varying the applied magnetic field direction. These differences may distinguish the origin of topological magnon gaps in CrI₃ and other van der Waals magnetic layers. Our findings pave the way for exploration and engineering topological gaps in van der Waals materials.

I. INTRODUCTION

With the experimental demonstration of long-range magnetic order in two-dimensional (2D) van der Waals (vdW) materials [1–3], 2D magnetic materials have come into focus [4–15]. Among them, ferromagnetic CrI₃ with a honeycomb lattice structure [16] has been attracting intense interest. The experimental observation of a gap opening in the Dirac-like magnon spectrum at the K symmetry points of ferromagnetic CrI₃ layers [17] has triggered wide discussions about the microscopic origin of the gap opening. Several proposals have suggested that this gap possesses a topological character, originating from either the Dzyaloshinskii-Moriya (DM) [5,17–22] or Kitaev [20,21,23–28] interaction. In contrast, alternative theories have associated this gap with electron correlations and spin-phonon interactions, implying a nontopological origin [29,30].

The existence of a topological magnon gap gives rise to several interesting features and exotic phases in 2D magnetic systems, such as magnon Hall effects, topological magnon and Chern insulator phases, spin Hall effects for Weyl magnons, and magnonic Floquet topological insulators [14,31–34]. Therefore, it is essential to determine the microscopic origin of the magnon gap opening and the fundamental interactions that control this topological gap, opening a route to 2D materials with engineered dynamic properties.

In a recent experiment, it was demonstrated that the Dirac gap at the K points in CrI₃ layers remains open and nearly unchanged when an in-plane (IP) magnetic field is applied to induce an IP magnetization configuration [19]. Apparently, this observation is not compatible with theoretical models featuring next-nearest-neighbor (NNN) DM interactions with an out-of-plane (OOP) DM vector [35,36].

Furthermore, recent theoretical studies have shown that it is possible to alter the topological properties of ferromagnetic and antiferromagnetic systems by adjusting the magnetization direction [37–43]. Therefore, tuning the magnetic ground state using an external magnetic field might be a useful tool to explore the nature of topological magnon bands.

In this paper, we propose that an angular magnetic field–dependent analysis of the magnon dispersion relation, more specifically the Dirac gap size and the position of Dirac-like cones, can be used to discriminate between DM and Kitaev interaction mechanisms in CrI₃. We combine our analytical linear spin-wave theory at zero temperature with numerical results from atomistic spin dynamics simulations at finite but low temperature to study the angular magnetic field

174425-1

dependency of the magnon dispersion. We show that a tilted NNN DM vector may reproduce the results of the recent experiment better than a Kitaev model.

The rest of this paper is structured as follows. In Sec. II, we introduce the DM and Kitaev spin-model Hamiltonians and our theoretical and numerical methodology. In Sec. III, we show the angular-dependent magnon dispersion of these two spin models. In Sec. IV, we suggest relevant observations for examination in future experiments. Finally, we conclude in Sec. V.

II. MODEL

We aim to compare two proposed spin models for a 2D ferromagnetic insulator honeycomb lattice in CrI$_3$. Although a combined model is theoretically feasible in this system, our focus here is on investigating the distinct effects arising from each model.

Magnon branches in both models are anticipated to manifest a topological band gap at K and K' symmetry points of the Brillouin zone (BZ). In this paper, we use a Kitaev model, proposed in Ref. [23], and compare it with a DM model, proposed in Ref. [5], to describe the spin dynamics in CrI$_3$. For the Kitaev model, the spin-interaction Hamiltonian includes the bond-directional anisotropy given by [23]

$$\mathcal{H}_\kappa = -J_\kappa \sum_{\langle i,j \rangle} \mathbf{S}_i \cdot \mathbf{S}_j - D_z \sum_i \left(S_i^z \right)^2 - \mu_s h_0 \sum_i \mathbf{B} \cdot \mathbf{S}_i$$
$$- \kappa \sum_{\langle i,j \rangle \in \eta} S_i^\eta S_j^\eta, \tag{1}$$

while the spin-interaction Hamiltonian for the DM model reads [5]

$$\mathcal{H}_{\mathrm{DM}} = -\sum_{i<j} \left(J_{ij} \mathbf{S}_i \cdot \mathbf{S}_j + \lambda_{ij} S_i^z S_j^z \right) - D_z \sum_i \left(S_i^z \right)^2$$
$$- \mu_s h_0 \sum_i \mathbf{B} \cdot \mathbf{S}_i - K_{\mathrm{bq}} \sum_{\langle i,j \rangle} (\mathbf{S}_i \cdot \mathbf{S}_j)^2$$
$$- \sum_{\langle\langle i,j \rangle\rangle} \mathbf{A}_{ij} \cdot \mathbf{S}_i \times \mathbf{S}_j. \tag{2}$$

In the above Hamiltonians, $\mathbf{S}_i$ is a unit vector that carries the spin-moment direction at site i [44], $\mathbf{B}$ is the direction of the external magnetic field with strength h_0, μ_s is the atomic magnetic moment, and $D_z > 0$ is the OOP easy-axis magnetic anisotropy along the z direction. The symbols $\langle \dots \rangle$ and $\langle\langle \dots \rangle\rangle$ represent the sums over nearest neighbor (NN) and NNN sites, respectively. The direction of the magnetic field determines the ground-state magnetization direction when its amplitude is larger than a critical value, dictated by the magnetic anisotropy. In the Kitaev model, Eq. (1), J_κ represents the NN isotropic Heisenberg exchange interaction, and κ denotes the NN bond-η-dependent Kitaev interaction strength. In the DM model, Eq. (2), the bilinear Heisenberg exchange interaction is split into the isotropic J_{ij} and anisotropic λ_{ij} terms, and the sum runs over up to the third NNs. In this spin Hamiltonian, K_{bq} is the strength of the NN biquadratic exchange interaction, which renormalizes the isotropic Heisenberg exchange interactions, see Eq. (D6) in the Supplemental Material (SM) [45], and

$\mathbf{A}_{ij}^{\mathrm{NNN}} = \nu_{ij}(A_x^{\mathrm{NNN}} \hat{\mathbf{x}} + A_y^{\mathrm{NNN}} \hat{\mathbf{y}} + A_z^{\mathrm{NNN}} \hat{\mathbf{z}}) = \nu_{ij}(A, \theta_{\mathrm{DM}}, \varphi_{\mathrm{DM}})$ is the DM vector [20,22], with $\nu_{ij} = -\nu_{ji} = \pm 1$, $A = |\mathbf{A}_{ij}^{\mathrm{NNN}}|$, and θ_{DM} (φ_{DM}) is the polar (azimuthal) angle. For simplicity, we set $\varphi_{\mathrm{DM}} = 0$, which corresponds to the IP x direction, while the ground-state magnetization direction can vary in different directions with respect to the DM vector. The average magnetization direction of the ground state, $\mathbf{m} = N^{-1} \sum_i^N \mathbf{S}_i$, is a vector $\mathbf{m} = (1, \theta_m, \varphi_m)$ normalized to the unit length that can be controlled by an external magnetic field. We define the relative angle between the DM vector and the magnetization direction as $\theta = \theta_{\mathrm{DM}} - \theta_m$.

A. Magnon dispersion from linear spin-wave theory

We analytically calculate the noninteracting magnon dispersion for an arbitrary ground-state magnetization direction, determined by an external magnetic field, in both Kitaev and DM models. To compute the magnon dispersion relations, we use the standard linear spin-wave theory by applying the Holstein-Primakoff transformation [46] at zero temperature. The noninteracting magnon Hamiltonian in the second quantized representation reads

$$\mathcal{H}_{\kappa(\mathrm{DM})} = \sum_{\mathbf{q},\sigma} E_{\mathbf{q}\sigma}^{\kappa(\mathrm{DM})} a_{\mathbf{q},\sigma}^\dagger a_{\mathbf{q},\sigma}, \tag{3}$$

where $a_{\mathbf{q},\sigma}(a_{\mathbf{q},\sigma}^\dagger)$ is the bosonic annihilation (creation) operator for acousticlike $\sigma = -$ and opticallike $\sigma = +$ magnon modes with eigenenergy $E_{\mathbf{q}\sigma}^{\kappa(\mathrm{DM})}$. In the Kitaev (DM) model, a topological Dirac magnon gap can be opened at the K points depending on the tilting angle of the magnetization direction θ_m (the relative angle between the DM vector and magnetization θ), $\Delta_K^{\kappa(\mathrm{DM})} = E_{\mathbf{q}=K,\sigma=+}^{\kappa(\mathrm{DM})} - E_{\mathbf{q}=K,\sigma=-}^{\kappa(\mathrm{DM})}$.

In the OOP magnetization configuration, the DM model with an OOP DM vector leads to a topological magnon gap at the K points which is linearly proportional to the OOP DM strength $\Delta_K^{\mathrm{DM}}(\theta = 0) \approx A_z^{\mathrm{NNN}}$, while in the Kitaev model, the K-point gap depends on different spin interactions and, more importantly, on the external OOP magnetic field $\Delta_K^\kappa(\theta = 0) \approx t_0 - \sqrt{t_0^2 - \kappa^2(\frac{3}{2})^2}$, with $t_0 = (9J_\kappa + 3\kappa)/2 + \mu_s h_0$, with $\kappa, \mu_s h_0, J_\kappa \gg D_z$. From these topological magnon gap expressions, it is evident that, in the OOP magnetic state, unlike the DM-induced topological gap, the Kitaev-induced topological gap can be tuned by varying the strength of the OOP magnetic field [37]. In general, both the OOP easy-axis magnetic anisotropy and magnetic field strengths modify the topological gap value in the Kitaev model, see the SM [45].

Since the magnetic unit cell in a honeycomb lattice has two spins, there are two magnon branches in the CrI$_3$ single layer, as shown in Figure 1. The black dotted curves in Figure 1 show the analytical magnon dispersion for (a) the Kitaev and (b) the DM models. Note that, in the analytical calculations involving the DM Hamiltonian, Eq. (2), we solely consider the isotropic NN exchange interaction in the first term of the Hamiltonian. Including all NNs in the simulation of the atomistic spin model leads to a stretching of the acoustic branch and compression of the optic branch [5], as shown by the red lines.
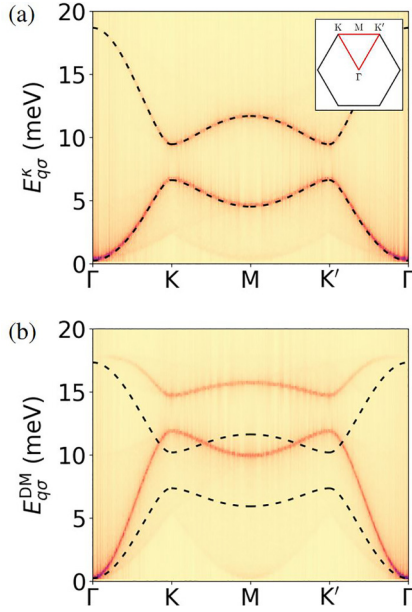
FIG. 1. Magnon dispersion of single-layer CrI_3 in the out-of-plane magnetization configuration in the absence of magnetic field as obtained from atomistic spin simulations (color map) and linear spin wave theory (black dashed lines). The parameters for (a) the Kitaev model and (b) the DM model can be found in the Supplemental Material [45]. Note that, in the Dzyaloshinskii-Moriya (DM) model, only first-nearest-neighbor (NN) exchange is included in the analytical model, while up to third NNs are included in the atomistic simulation. This leads to a stretching of the low-energy band and a compression of the high-energy band [5] but does not affect the size and position of the topological Dirac gap at the K and K' points.

Since the magnon dispersion expressions for arbitrary ground-state magnetization directions are lengthy, we only show a graphical representation of the results in the main text and refer to the SM [45] for the analytic expressions.

B. Magnon dispersion from atomistic spin-dynamics simulations

The dynamic of spins within our two models is simulated using the VAMPIRE software package [44,47] that solves the stochastic Landau-Lifshitz-Gilbert (sLLG) equation, applied at the atomistic level [44,48], numerically. The sLLG equation reads

$$\frac{\partial \mathbf{S}_i}{\partial t} = -\frac{\gamma}{1+\alpha^2}\left\{\mathbf{S}_i \times \mathbf{B}_i^{\kappa(\mathrm{DM})} + \alpha \mathbf{S}_i \times \left[\mathbf{S}_i \times \mathbf{B}_i^{\kappa(\mathrm{DM})}\right]\right\}, \quad (4)$$

where γ is the electron gyromagnetic ratio, and α is the Gilbert damping constant. The effective magnetic field for theKitaev (DM) model $\mathbf{B}_i^{\kappa(\mathrm{DM})} = -\mu_s^{-1}\partial\mathcal{H}_{\kappa(\mathrm{DM})}/\partial\mathbf{S}_i + \boldsymbol{\xi}_i^{(\mathrm{th})}$ consists of a deterministic contribution from the corresponding spin-interaction Hamiltonian, the first term, and a stochastic thermal field, the second term. The latter introduces temperature to the system and is modeled by an uncorrelated Gaussian thermal noise that obeys

$$\left\langle \boldsymbol{\xi}_i^{(\mathrm{th})}(t) \right\rangle = 0, \quad (5a)$$

$$\left\langle \xi_{i,m}^{(\mathrm{th})}(t)\xi_{j,n}^{(\mathrm{th})}(t') \right\rangle = 2\alpha k_\mathrm{B} T \gamma^{-1}\mu_s^{-1}\delta_{ij}\delta_{mn}\delta(t-t'), \quad (5b)$$

where $m, n = \{x, y, z\}$ represent spatial components, and k_B is the Boltzmann constant.

To simulate spin dynamics in single-layer CrI_3, we consider a honeycomb lattice with a size of 300×300 unit cells, $\sim 1.8 \times 10^5$ spins, at low but finite temperature. A preconditioning adaptive-step Monte Carlo simulation is employed to achieve thermal equilibrium within the system [49]. To ensure rapid convergence, the damping constant α is set to 1 during the preconditioning. In the next step, we integrate the stochastic Langevin Equation (4) dynamically using a stochastic Heun method [44] over 30 ps, with a time step of 5 fs, and damping $\alpha = 0.01$. This choice of time step, along with low damping, is sufficient to obtain accurate magnon spectra [50,51]. The magnon spectra for a path in momentum space can be derived by computing the fast Fourier transform of spatially and temporally dependent spin-moment directions. For more details, see the SM [45].

At low temperatures, the density of thermal magnons is low, and nonlinear magnon interactions are comparatively weak. As temperatures increase, these nonlinear interactions may give rise to topological phase transitions [52].

The magnon spectra obtained from the atomistic spin-dynamics simulations at low temperatures closely align with the predictions of the linear spin-wave theory at zero temperature, as shown for the OOP magnetization configuration in Figure 1 and various orientations of the ground-state magnetization in the SM [45].

III. ENGINEERING OF THE MAGNON DISPERSION RELATION

In this section, we employ the numerical and analytical methods outlined in the previous section to investigate the impact of the magnetization direction on the magnon spectra for the two proposed spin models of CrI_3.

A. Migration of the Dirac gap in the Kitaev model

The previously introduced Kitaev model in Eq. (1) successfully replicates the experimentally observed magnon band gap at the Γ point and Dirac points, as reported in Ref. [19]. This is achieved by employing the following spin parameters: $J = 0.55\,\mathrm{meV}$, $\kappa = 4.5\,\mathrm{meV}$, and $D_z = 0.1\,\mathrm{meV}$.

The Kitaev interaction κ opens a Dirac gap at the K and K' points, as presented in Figure 1(a), where the magnon dispersion is shown for an OOP magnetization ground state. In this figure, we compare numerical results from atomistic spin simulations at low temperature, indicated by the color map, with analytical results from linear spin-wave theory at zero temperature, drawn with the black dashed line. We find excellent agreement between both methods and that the Γ and K point gaps are comparable with the experimental values [17,19].

In Figure 2(a), we present constant-energy cuts of the magnon dispersion for the OOP magnetization direction. Here, the Dirac-like cones sit at the K and K' points because of C_{3v} symmetry [53,54]. However, when rotating the magnetization direction to the IP configuration, e.g., along the x direction, although the Dirac gaps remain open, the Dirac cones are displaced from the high-symmetry K and K' points,
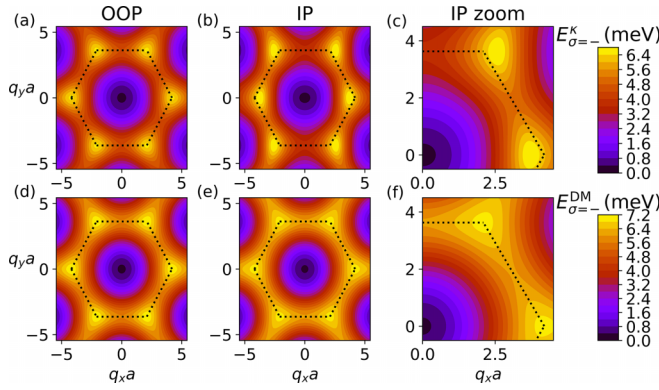
FIG. 2. Analytic comparison of the positions of the Dirac-like cones in the magnon dispersion relation at out-of-plane (OOP, left column) and in-plane (IP, right columns) orientation with constant-energy cuts. In the Kitaev (κ) model, the Dirac-like cones are at the K points in (a)the OOP configuration but migrate into (b) and (c) the IP configuration. In contrast, (d)–(f) in the Dzyaloshinskii-Moriya (DM) model with a tilted DM vector, the cones remain at the K points. Here, the low-energy band $\sigma = -$ is shown, and the color map scales from blue (low energy) to red and yellow (high energy). The magnetic field strength is 4.5 T [19].

see Figs. 2(b) and 2(c). The two Dirac cones along the $q_y = 0$ line migrate toward the center of the BZ, while the other four Dirac cones, with finite q_y, move outward from the original BZ. Hence, the BZ is squeezed along the y direction when spins are along the x direction in this model. If the IP magnetization direction is set along the y direction, the BZ is squeezed along the x direction (not shown). This displacement of the Dirac cones should be distinguished from recently reported intensity widening [19] and Dirac nodal lines [19,27,55].

While the magnetic field direction moves the Dirac points, the magnetic field strength modifies the Dirac gap size, which will be discussed below.

B. Tuning of the Dirac gap size in the DM model

To investigate magnon dispersion relations in the DM model in Eq. (2), we use the spin-interaction parameters reported in Ref. [5], which are listed in the SM [45]. However, since a magnon gap is only opened at Dirac points if the ground-state magnetization direction has a finite projection on the NNN DM vector, i.e., $\mathbf{A} \cdot \mathbf{m} \neq 0$ or $\theta \neq 90°$, we argue that the NNN DM vector must be tilted. Only when the NNN DM vector is tilted can a finite magnon gap be opened in both OOP and IP magnetic configurations, as observed in recent magnon dispersion measurements in Ref. [19].

In a pristine magnetic layer with honeycomb lattice structure, the intrinsic NNN DM vector is perpendicular to the plane [56] by the constraints of symmetry. However, we argue that, in realistic layered vdW magnetic materials, such as CrI$_3$, this intrinsic DM vector might be tilted by reducing the lattice symmetry due to various reasons. First, a single layer of these magnetic materials consists of several nonmagnetic atomic layers that break the mirror and inversion symmetries [18,57]. In the case of monolayer CrI$_3$, the magnetic Cr ions arrange themselves in a honeycomb lattice, where each Cr atom is surrounded by six I atoms, creating a distorted octahedral
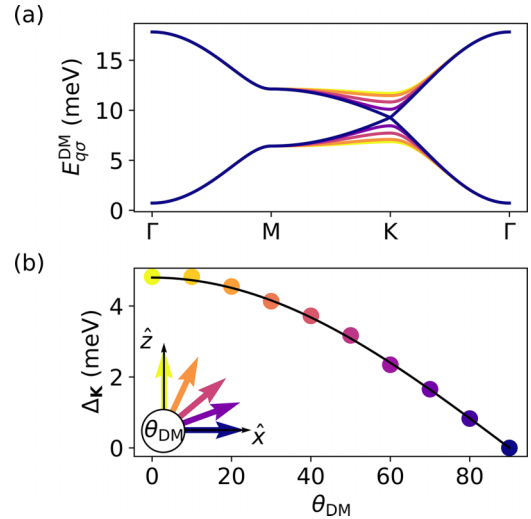

FIG. 3. Impact of Dzyaloshinskii-Moriya (DM) interaction on the magnon dispersion relation in the out-of-plane magnetization configuration. (a) Tilting the DM vector only impacts the edge of the Brillouin zone (BZ). The gap size is read out and presented below. (b) When the relative angle θ_{DM} between the DM vector and the magnetization direction increases from parallel $\theta_{DM} = 0°$ (yellow) to orthogonal $\theta_{DM} = 90°$ (blue), the gap at the K symmetry point Δ_K closes. The numerical results shown as points agree with the analytical result $\Delta_K^{DM}(\theta_{DM}) = \Delta_K^{DM}(0) \cos\theta_{DM}$, drawn with the black line, where $\Delta_K^{DM}(0) = 9\sqrt{3}A$.

structure through edge sharing. Second, strain can induce lattice distortion and/or inversion symmetry breaking [57–60]. The strain can be externally applied or caused by growing CrI$_3$ on a substrate. Third, it is worth noting that magnon dispersions have, thus far, been measured exclusively in multilayered vdW systems and not in a truly single magnetic layer. This may lead to the deviation of the NNN DM vector from the OOP direction by inversion symmetry breaking [20].

In Figure 3, we show how tilting the DM vector changes the value of the magnon gap at the K point when the magnetic ground state is OOP $\theta_m = 0$. It is evident from Figure 3(a) that the direction of the DM vector only has an impact at the edges of the BZ. The analytical linear spin-wave theory is in perfect agreement with the magnon dispersion computed numerically, see the SM [45]. The size of the magnon gap at the K point, depending on the DM angle $\Delta_K(\theta_{DM})$, is read out and presented in Figure 3(b) with colored points for the numerical solution and the solid black line for the analytical solution. At $\theta_{DM} = 0°$ (yellow), where the magnetization direction and the DM vector are parallel, the magnon band gap at the high-symmetry K and K' points is maximal. With increasing angle between the magnetization and the DM vector, the gap reduces, until at $\theta_{DM} = 90°$ (blue), where the magnetization direction and the DM vector are orthogonal and the magnon band gap at the high-symmetry K and K' points is closed.

Assuming a DM strength of $A \approx 0.31$ meV as reported in Ref. [5], we find that a DM tilting angle of $\theta_{DM} = 54°$ reproduces the reported magnon band gap at the K point $\Delta_K \approx 2.8$ meV, in Ref. [19]. It should be stressed that only the magnitude of the DM interaction and the relative orientation

between the DM vector and the magnetization direction is relevant for the size of the magnon gap at Dirac points. Through the application of an external magnetic field and the rotation of the CrI_3 sample, it becomes feasible to experimentally engineer the DM-induced topological band gap. In the DM model, in contrast to the Kitaev model, the Dirac cones remain at the K and K' points for both OOP and IP magnetization, see Figs. 2(d)–2(f).

IV. DISCUSSION AND PROPOSAL

In Figure 2, we present a comparative analysis of constant-energy cuts of magnon dispersion within the BZ for IP and OOP magnetic geometries in both Kitaev [Figs. 2(a)–2(c)] and DM [Figs. 2(d)–2(f)] models. In all subplots, the BZ of a hexagonal lattice is depicted for comparison. For an OOP magnetization ground state, Figs. 2(a) and 2(d), all Dirac-like cones are at the K and K' points in both Kitaev and DM models. However, with an IP magnetization ground state, Figs. 2(b), 2(c), 2(e), and 2(f), although the Dirac-like cones remain at the K and K' points in the DM model, they shift in the Kitaev model.

We propose that two quantities must be experimentally investigated under variation of the ground-state magnetization direction θ_m: first, the size of the band gap at the K and K' points Δ_K, and second, the position of the Dirac-like cones $\mathbf{k}_{DC}^\sigma$ with respect to the K and K' points, ($|\mathbf{k}_{DC}^\sigma - \mathbf{K}|a$), for each magnon branch σ.

In Figure 4(a), we compare the angular dependence θ_m of the topological magnon gap at the K point $\Delta_K(\theta_m)$ for the DM model with a tilted DM vector (black solid line) and the Kitaev model (green dashed line). In our model, the DM vector is tilted by $54°$. Consequently, the Dirac gap remains open for both OOP with $\theta_m = 0$ and IP with $\theta_m = 90°$ magnetization directions. As previously discussed, the Dirac gap closing is influenced by the relative angle between the NNN DM vector and the magnetization direction. Although our spin-model parameters used in both Kitaev and the DM models reproduce a topological magnon gap at IP and OOP magnetization directions comparable with the recent experimental data [19], the angular dependence of them is quite different. In the Kitaev model, the magnon gap at the K and K' points Δ_K varies with the external magnetic field direction but never closes. On the contrary, in the DM model with tilted DM vector, the topological gap is largest when the ground state magnetization and DM vector are parallel and closes when magnetization and DM vector are orthogonal. In Figure 4(a), four angles are indicated with vertical dashed lines that are characteristic for our model.

As we mentioned before, the magnon Dirac-like cones in the DM model remain at the K and K' points for all magnetization directions. In contrast, in the Kitaev model, the Dirac cones are displaced by varying the magnetization direction. This can be explained in terms of threefold rotational symmetry about the z axis, the C_{3z} spin point group symmetry [61]. In the OOP configuration, both the Kitaev and DM interactions preserve this symmetry, and the Dirac points remain at the K and K' points. However, with IP magnetization, the Kitaev interaction breaks C_{3z} symmetry, which allows the Dirac points to move away from the K and K' points. On the other hand,
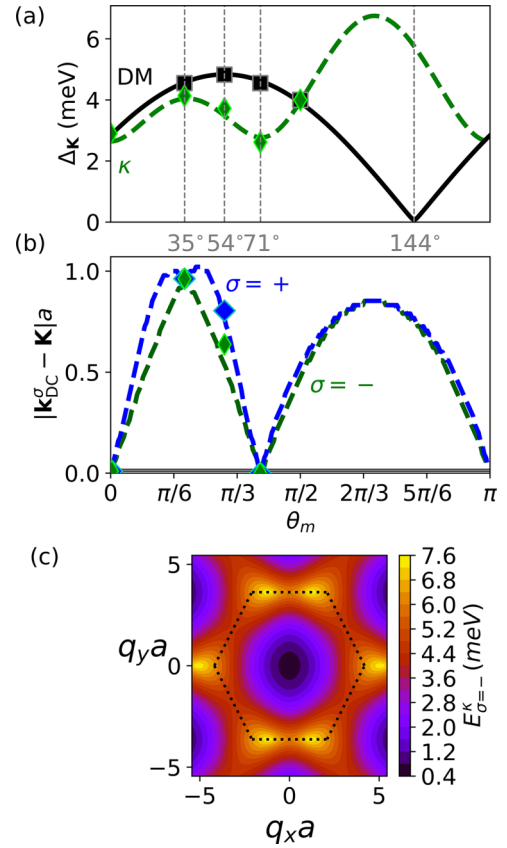

FIG. 4. Impact of the tilting angle θ_m on dispersion, from out-of-plane (OOP, $\theta_m = 0$) over in-plane (IP, $\theta_m = \pi/2$) to negative OOP ($\theta_m = \pi$). Solid lines are obtained analytically within linear spin-wave theory and in agreement with numerical data, obtained from atomistic simulations, for selected angles, shown with squares for the Dzyaloshinskii-Moriya (DM) model and diamonds for the Kitaev model. (a) Gap at the K point Δ_K for the Kitaev (green dashed) and DM (black solid) models dependent on the magnetization direction θ_m. The DM direction is fixed at $54°$. (b) Displacement of the Dirac-like cones at $\mathbf{k}_{DC}^\sigma$ from the K point in the acoustic ($\sigma = -$) and optic ($\sigma = +$) branches for the Kitaev (green dashed lines) and DM (black and gray solid lines, both remaining zero) models. Characteristic angles indicated by vertical lines. (c) Constant-energy cut in the Kitaev model at $\theta_m = 35°$ showing the migration of the Dirac gap. For tilting the magnetization, a magnetic field of 4.5 T is applied [19].

in the DM model, C_{3z} symmetry is preserved even when there is a finite angle between the DM vector and the magnetization direction, fixing the Dirac points to the K and K' points [61].

Furthermore, there are several direct-indirect band gap transitions in the magnon spectra. In Figure 4(b), the position of the Dirac cones $\mathbf{k}_{DC}^\sigma$ with respect to K and K' points are shown for each branch σ in both models. In the DM model (gray and black lines), the cones remain at the K point, and the magnon band gap is always direct. However, in the Kitaev model, shown by dashed green and blue lines, we observe a significant displacement of cones with maximal displacement around $\theta_m = 35°$. In addition, as shown by a different amplitude of displacement for the two branches, the band gap is indirect where the blue ($\sigma = +$) and green ($\sigma = -$) branches overlap. To illustrate the displacement of the Dirac

gap in the Kitaev model, a constant-energy cut is presented in Figure 4(c) for $\theta_m = 35°$, clearly showing a migration of the Dirac cones away from the K and K' points. In Figs. 4(a) and 4(b), we find good agreement between our analytical solution, shown with solid lines, and the numerical results at selected angles, shown with markers. Our atomistic spin simulations reproduce all crucial features: the changing topological magnon gap size for both models as well as a shift in the Dirac cone positions and a direct-indirect gap transition in the Kitaev model.

We have numerically tested a combined model that includes both Kitaev and DM interactions and find that the two mechanisms cooperate in the Dirac gap opening, but only the Kitaev interaction determines the Dirac cone position.

To test our predictions—that the dominant mechanism of opening the topological magnon gap at the Dirac points of CrI$_3$ is the DM interaction, and the Kitaev interaction is negligible—we propose measuring the magnon dispersion at varying external magnetic field angles. By comparing the topological gap values and the shift of the Dirac-like cones, we can determine whether the DM or Kitaev interaction is the primary mechanism responsible for the topological gap opening at the Dirac points.

So far, we have examined only the effect of the magnetic field direction, equivalent to the magnetization direction, on the magnon dispersion. However, we have already mentioned that the size of the magnon gap at the Dirac points in the Kitaev model also depends on the amplitude of the magnetic field, as also predicted in Ref. [37]. Thus, we suggest the analysis of the gap value in the presence of an OOP magnetic field as an another possible experimental study. For example, applying an external magnetic field of 9 T in the OOP direction, the gap would decrease by 0.36 meV ($\sim$13%) compared with the case without the magnetic field. It is worth pointing out that the magnetic field strength does not have an impact on the migration of the Dirac cones, and thus, the characteristic external magnetic field angles that are indicated in Figure 4(a) remain unchanged.

V. OUTLOOK

We have reexamined the unresolved issue regarding the microscopic origin of the topological magnon band gap observed experimentally at the high-symmetry K and K' points of ferromagnetic CrI$_3$ single layers. This investigation involves a comparison of the angular dependence of the Dirac magnon gap size and its position in the DM model and the Kitaev model. We have shown that, in the Kitaev approach, the size and position of the Dirac points are related to the amplitude and orientation of an applied magnetic field. In contrast, in the DM model, the magnon band gap is related to the angle between the ground-state magnetization direction and the NNN DM vector. We propose that a tilted DM vector may explain recent magnon dispersion measurements in CrI$_3$ layers [19] and motivate further experimental work to engineer intrinsic nontrivial interactions. Based on our findings, we suggest that experimentally exploring the angular dependence of the magnon gap will not only serve as a valuable route to investigate its microscopic origin but also offer a clear pathway to manipulate and tailor topological gaps on-demand accordingly with the target applications.

[1] C. Gong, L. Li, Z. Li, H. Ji, A. Stern, Y. Xia, T. Cao, W. Bao, C. Wang, Y. Wang *et al.*, Discovery of intrinsic ferromagnetism in two-dimensional van der Waals crystals, Nature (London) **546**, 265 (2017).

[2] J.-U. Lee, S. Lee, J. H. Ryoo, S. Kang, T. Y. Kim, P. Kim, C.-H. Park, J.-G. Park, and H. Cheong, Ising-type magnetic ordering in atomically thin FePS$_3$, Nano Lett. **16**, 7433 (2016).

[3] X. Wang, K. Du, Y. Y. F. Liu, P. Hu, J. Zhang, Q. Zhang, M. H. S. Owen, X. Lu, C. K. Gan, P. Sengupta *et al.*, Raman spectroscopy of atomically thin two-dimensional magnetic iron phosphorus trisulfide (FePS$_3$) crystals, 2D Mater. **3**, 031009 (2016).

[4] D. A. Wahab, M. Augustin, S. M. Valero, W. Kuang, S. Jenkins, E. Coronado, I. V. Grigorieva, I. J. Vera-Marun, E. Navarro-Moratalla, R. F. L. Evans *et al.*, Quantum rescaling, domain metastability, and hybrid domain-walls in 2D CrI$_3$ magnets, Adv. Mater. **33**, 2004138 (2021).

[5] A. Kartsev, M. Augustin, R. F. L. Evans, K. S. Novoselov, and E. J. G. Santos, Biquadratic exchange interactions in two-dimensional magnets, npj Comput. Mater. **6**, 150 (2020).

[6] C. Tang, L. Alahmed, M. Mahdi, Y. Xiong, J. Inman, N. J. McLaughlin, C. Zollitsch, T. H. Kim, C. R. Du, H. Kurebayashi *et al.*, Spin dynamics in van der Waals magnetic systems, Phys. Rep. **1032**, 1 (2023).

[7] Q. H. Wang, A. Bedoya-Pinto, M. Blei, A. H. Dismukes, A. Hamo, S. Jenkins, M. Koperski, Y. Liu, Q.-C. Sun, E. J. Telford *et al.*, The magnetic genome of two-dimensional van der Waals materials, ACS Nano **16**, 6960 (2022).

[8] C. Boix-Constant, S. Jenkins, R. Rama-Eiroa, E. J. G. Santos, S. Mañas-Valero, and E. Coronado, Multistep magnetization switching in orthogonally twisted ferromagnetic monolayers, Nat. Mater. **23**, 212 (2024).

[9] Y. Zur, A. Noah, C. Boix-Constant, S. Mañas-Valero, N. Fridman, R. Rama-Eiroa, M. E. Huber, E. J. G. Santos, E. Coronado, and Y. Anahory, Magnetic imaging and domain nucleation in CrSBr down to the 2D limit, Adv. Mater. **35**, 2307195 (2023).

[10] B. W. Casas, Y. Li, A. Moon, Y. Xin, C. McKeever, J. Macy, A. K. Petford-Long, C. M. Phatak, E. J. G. Santos, E. S. Choi *et al.*, Coexistence of merons with skyrmions in the centrosymmetric van der Waals ferromagnet $Fe_{5-x}GeTe_2$, Adv. Mater. **35**, 2212087 (2023).

[11] S. Jenkins, L. Rózsa, U. Atxitia, R. F. L. Evans, K. S. Novoselov, and E. J. G. Santos, Breaking through the Mermin-Wagner limit in 2D van der Waals magnets, Nat. Commun. **13**, 6917 (2022).

[12] M. Daąbrowski, S. Guo, M. Strungaru, P. S. Keatley, F. Withers, E. J. G. Santos, and R. J. Hicken, All-optical control of spin in a 2D van der Waals magnet, Nat. Commun. **13**, 5976 (2022).

[13] M. Khela, M. Daąbrowski, S. Khan, P. S. Keatley, I. Verzhbitskiy, G. Eda, R. J. Hicken, H. Kurebayashi, and E. J. G. Santos, Laser-induced topological spin switching in a 2D van der Waals magnet, Nat. Commun. **14**, 1378 (2023).

[14] Y.-M. Li, Y.-J. Wu, X.-W. Luo, Y. Huang, and K. Chang, Higher-order topological phases of magnons protected by magnetic crystalline symmetries, Phys. Rev. B **106**, 054403 (2022).

[15] H. Iturriaga, L. M. Martinez, T. T. Mai, A. J. Biacchi, M. Augustin, A. R. Hight Walker, M. F. Sanad, S. T. Sreenivasan, Y. Liu, E. J. G. Santos *et al.*, Magnetic properties of intercalated quasi-2D $Fe_{3-x}GeTe_2$ van der Waals magnet, npj 2D Mater. Appl. **7**, 56 (2023).

[16] B. Huang, G. Clark, E. Navarro-Moratalla, D. R. Klein, R. Cheng, K. L. Seyler, D. Zhong, E. Schmidgall, M. A. McGuire, D. H. Cobden *et al.*, Layer-dependent ferromagnetism in a van der Waals crystal down to the monolayer limit, Nature (London) **546**, 270 (2017).

[17] L. Chen, J.-H. Chung, B. Gao, T. Chen, M. B. Stone, A. I. Kolesnikov, Q. Huang, and P. Dai, Topological spin excitations in honeycomb ferromagnet CrI_3, Phys. Rev. X **8**, 041028 (2018).

[18] C. Xu, J. Feng, S. Prokhorenko, Y. Nahas, H. Xiang, and L. Bellaiche, Topological spin texture in Janus monolayers of the chromium trihalides $Cr(I, X)_3$, Phys. Rev. B **101**, 060404(R) (2020).

[19] L. Chen, J.-H. Chung, M. B. Stone, A. I. Kolesnikov, B. Winn, V. O. Garlea, D. L. Abernathy, B. Gao, M. Augustin, E. J. G. Santos *et al.*, Magnetic field effect on topological spin excitations in CrI_3, Phys. Rev. X **11**, 031047 (2021).

[20] M. Soenen, C. Bacaksiz, R. M. Menezes, and M. V. Milošević, Stacking-dependent topological magnons in bilayer CrI_3, Phys. Rev. Mater. **7**, 024421 (2023).

[21] R. Jaeschke-Ubiergo, E. Suárez Morell, and A. S. Nunez, Theory of magnetism in the van der Waals magnet CrI_3, Phys. Rev. B **103**, 174410 (2021).

[22] D. Šabani, C. Bacaksiz, and M. V. Milošević, *Ab initio* methodology for magnetic exchange parameters: Generic four-state energy mapping onto a Heisenberg spin Hamiltonian, Phys. Rev. B **102**, 014457 (2020).

[23] I. Lee, F. G. Utermohlen, D. Weber, K. Hwang, C. Zhang, J. van Tol, J. E. Goldberger, N. Trivedi, and P. C. Hammel, Fundamental spin interactions underlying the magnetic anisotropy in the Kitaev ferromagnet CrI_3, Phys. Rev. Lett. **124**, 017201 (2020).

[24] C. Xu, J. Feng, H. Xiang, and L. Bellaiche, Interplay between Kitaev interaction and single ion anisotropy in ferromagnetic CrI_3 and $CrGeTe_3$ monolayers, npj Comput. Mater. **4**, 57 (2018).

[25] P. P. Stavropoulos, X. Liu, and H.-Y. Kee, Magnetic anisotropy in spin-$\frac{3}{2}$ with heavy ligand in honeycomb Mott insulators: Application to CrI_3, Phys. Rev. Res. **3**, 013216 (2021).

[26] E. Aguilera, R. Jaeschke-Ubiergo, N. Vidal-Silva, L. E. F. F. Torres, and A. S. Nunez, Topological magnonics in the two-dimensional van der Waals magnet CrI_3, Phys. Rev. B **102**, 024409 (2020).

[27] M. Elliot, P. A. McClarty, D. Prabhakaran, R. D. Johnson, H. C. Walker, P. Manuel, and R. Coldea, Order-by-disorder from bond-dependent exchange and intensity signature of nodal quasiparticles in a honeycomb cobaltate, Nat. Commun. **12**, 3936 (2021).

[28] J. Cen and H.-Y. Kee, Determining Kitaev interaction in spin-S honeycomb Mott insulators, Phys. Rev. B **107**, 014411 (2023).

[29] L. Ke and M. I. Katsnelson, Electron correlation effects on exchange interactions and spin excitations in 2D van der Waals materials, npj Comput. Mater. **7**, 4 (2021).

[30] P. Delugas, O. Baseggio, I. Timrov, S. Baroni, and T. Gorni, Magnon-phonon interactions enhance the gap at the Dirac point in the spin-wave spectra of CrI_3 two-dimensional magnets, Phys. Rev. B **107**, 214452 (2023).

[31] P. A. McClarty, Topological magnons: A review, Annu. Rev. Condens. Matter Phys. **13**, 171 (2022).

[32] V. A. Zyuzin and A. A. Kovalev, Spin Hall and Nernst effects of Weyl magnons, Phys. Rev. B **97**, 174407 (2018).

[33] S. A. Owerre, Floquet topological magnons, J. Phys. Commun. **1**, 021002 (2017).

[34] A. T. Costa, D. L. R. Santos, N. M. R. Peres, and J. Fernández-Rossier, Topological magnons in CrI_3 monolayers: An itinerant fermion description, 2D Mater. **7**, 045031 (2020).

[35] S. A. Owerre, A first theoretical realization of honeycomb topological magnon insulator, J. Phys.: Condens. Matter **28**, 386001 (2016).

[36] S. K. Kim, H. Ochoa, R. Zarzuela, and Y. Tserkovnyak, Realization of the Haldane-Kane-Mele model in a system of localized spins, Phys. Rev. Lett. **117**, 227201 (2016).

[37] L.-C. Zhang, F. Zhu, D. Go, F. R. Lux, F. J. dos Santos, S. Lounis, Y. Su, S. Blügel, and Y. Mokrousov, Interplay of Dzyaloshinskii-Moriya and Kitaev interactions for magnonic properties of Heisenberg-Kitaev honeycomb ferromagnets, Phys. Rev. B **103**, 134414 (2021).

[38] B. Ma and G. A. Fiete, Antiferromagnetic insulators with tunable magnon-polaron Chern numbers induced by in-plane optical phonons, Phys. Rev. B **105**, L100402 (2022).

[39] P. Shen and S. K. Kim, Magnetic field control of topological magnon-polaron bands in two-dimensional ferromagnets, Phys. Rev. B **101**, 125111 (2020).

[40] G. Go and S. K. Kim, Tunable large spin Nernst effect in a two-dimensional magnetic bilayer, Phys. Rev. B **106**, 125103 (2022).

[41] G. Go, S. K. Kim, and K.-J. Lee, Topological magnon-phonon hybrid excitations in two-dimensional ferromagnets with tunable Chern numbers, Phys. Rev. Lett. **123**, 237207 (2019).

[42] J. N. Kløgetvedt and A. Qaiumzadeh, Tunable topological magnon-polaron states and anomalous Hall phenomena in two-dimensional ferromagnetic insulators, Phys. Rev. B **108**, 224424 (2023).

[43] M. Soenen and M. V. Milošević, Tunable magnon topology in monolayer CrI_3 under external stimuli, Phys. Rev. Mater. **7**, 084402 (2023).

[44] R. F. L. Evans, W. J. Fan, P. Chureemart, T. A. Ostler, M. O. A. Ellis, and R. W. Chantrell, Atomistic spin model simulations of magnetic nanomaterials, J. Phys.: Condens. Matter **26**, 103202 (2014).

[45] See Supplemental Material at http://link.aps.org/supplemental/10.1103/PhysRevB.109.174425 for the following information (1) Material parameters, (2) A detailed comparison of analytical with numerical results, (3) Supplementary angle-dependent results for both models, (4) Details about the analytic and numerical procedure for finding the dispersion relations.

[46] T. Holstein and H. Primakoff, Field dependence of the intrinsic domain magnetization of a ferromagnet, Phys. Rev. **58**, 1098 (1940).

[47] VAMPIRE software package v5 available from https://vampire.york.ac.uk/ (2020).

[48] M. O. A. Ellis, R. F. L. Evans, T. A. Ostler, J. Barker, U. Atxitia, O. Chubykalo-Fesenko, and R. W. Chantrell, The Landau-Lifshitz equation in atomistic models, Low Temp. Phys. **41**, 705 (2015).

[49] J. D. Alzate-Cardona, D. Sabogal-Suárez, R. F. L. Evans, and E. Restrepo-Parra, Optimal phase space sampling for Monte Carlo simulations of Heisenberg spin systems, J. Phys.: Condens. Matter **31**, 095802 (2019).

[50] C. Etz, L. Bergqvist, A. Bergman, A. Taroni, and O. Eriksson, Atomistic spin dynamics and surface magnons, J. Phys.: Condens. Matter **27**, 243202 (2015).

[51] J. Barker and G. E. W. Bauer, Thermal spin dynamics of Yttrium iron garnet, Phys. Rev. Lett. **117**, 217201 (2016).

[52] Y.-S. Lu, J.-L. Li, and C.-T. Wu, Topological phase transitions of Dirac magnons in honeycomb ferromagnets, Phys. Rev. Lett. **127**, 217202 (2021).

[53] J. L. Mañes, F. Guinea, and M. A. H. Vozmediano, Existence and topological stability of fermi points in multilayered graphene, Phys. Rev. B **75**, 155424 (2007).

[54] E. Kogan, Why Dirac points in graphene are where they are? arXiv:1112.3826.

[55] S. S. Pershoguba, S. Banerjee, J. C. Lashley, J. Park, H. Ågren, G. Aeppli, and A. V. Balatsky, Dirac magnons in honeycomb ferromagnets, Phys. Rev. X **8**, 011010 (2018).

[56] J. M. Losada, A. Brataas, and A. Qaiumzadeh, Ultrafast control of spin interactions in honeycomb antiferromagnetic insulators, Phys. Rev. B **100**, 060410(R) (2019).

[57] S. I. Vishkayi, Z. Torbatian, A. Qaiumzadeh, and R. Asgari, Strain and electric-field control of spin-spin interactions in monolayer CrI$_3$, Phys. Rev. Mater. **4**, 094004 (2020).

[58] A. Edström, D. Amoroso, S. Picozzi, P. Barone, and M. Stengel, Curved magnetism in CrI$_3$, Phys. Rev. Lett. **128**, 177202 (2022).

[59] K. Basak, M. Ghosh, S. Chowdhury, and D. Jana, Theoretical studies on electronic, magnetic and optical properties of two dimensional transition metal trihalides, J. Phys.: Condens. Matter **35**, 233001 (2023).

[60] H. Ren and G. Xiang, Strain engineering of intrinsic ferromagnetism in 2D van der Waals materials, Nanomaterials **13**, 2378 (2023).

[61] A. Corticelli, R. Moessner, and P. A. McClarty, Spin-space groups and magnon band topology, Phys. Rev. B **105**, 064430 (2022).

[62] http://www.cirrus.ac.uk.